T.Subamathi, et. al. International Journal of Engineering Research and Applications
www.ijera.com
ISSN: 2248-9622, Vol. 15, Issue 9, September 2025, pp 127-145

RESEARCH ARTICLE OPEN ACCESS

An Incredible YOLOv8 with Pixel-Level Fourth-Order Entropy Guided Class Activation Map Attention for Leukemia Detection and Classification

T.Subamathi*, N.A.Sheela Selvakumari **
**Department of Computer Science, PSGR Krishnammal College for Women, Coimbatore, Tamil Nadu,India*
Email: subaaa2398phd@gmail.com
*** Department of Computer Science, Sri Krishna Arts and Science College, Coimbatore, Tamil Nadu,India*
Email: mailsheela83@gmail.com

ABSTRACT
Leukemia, characterized by abnormal white blood cell development, is challenging to diagnose due to its wide range of signs and fast-changing condition. To improve patient outcomes and ensure successful medication, early and precise detection is critical. Traditional blood cancer detection methods may rely on subjective interpretations, delaying diagnosis until symptoms appear. Machine learning (ML) can detect patterns early and distinguish invisible patterns, making it a more accurate alternative. ML methods, however, have challenges with huge datasets and need careful feature selection. Leukemia detection methods have been refined by recent developments in Deep Learning (DL). One of them is a low-weight YOLOv8 model that contains a residual attention mechanism, which is designed to enhance the performance of leukemia detection and classification. To improve feature extraction and contextual information collection, this model was built by superimposing Residual Convolution Block Attention Mechanism (RCBAM) and Depthwise Separable Convolution (DWSCNN) layers on top of YOLOv8n architecture. However, while RCBAM can highlight relevant features, it is also possible for it to assign high weights to redundant or irrelevant features, potentially hindering performance. This paper proposes an advanced attention mechanism using Explainable AI (XAI) model. The capacity of XAI methods can disclose the reasoning behind network. The proposed explainable AI based attention mechanism is developed by integrating a Pixel-Level Fourth-Order Entropy guided Class Activation Map (PLFOECAM). In this work, fourth-order entropy information is leveraged to enhance Class Activation Maps (CAMs). To create feature map weights, entropy values are used instead of the conventional gradient averaging method. Since entropy is used directly to weight and sum feature maps, gradient-based approaches are not relied upon as much, which helps with the reliability of the CAM model. To identify and classify leukemia, the whole thing is called YOLOv8 with PLFOECAM Attention (YPALDC). Finally, the experimental results prove that the proposed model perform achieves 93.85%, 90.42% and 91.87% on SN-AM dataset, MiMM_SBILab Dataset, C-NMC dataset outperforming other standard models.

Keywords - Class Activation Map, Deep Learning, Machine Learning, Leukemia, YOLOv8

Date of Submission: 07-09-2025 Date of acceptance: 18-09-2025

I. INTRODUCTION

Leukemia refers to a malignant disorder of hematopoietic origin, characterized by abnormal proliferation of immature blood cells [1]. This unregulated expansion leads to overcrowding of the bone marrow, thereby inhibiting the formation of functional erythrocytes, leukocytes, and platelets, which are needed for oxygen carriage, immune function and coagulation [2]. As a result, patients often exhibit symptoms such as persistent fatigue, recurrent infections, pale complexion, excessive bruising, and unexplained bleeding, which typically worsen as the disease progresses [3].

Leukemia is broadly classified into four major types: acute lymphoblastic leukemia (ALL) [5], acute myeloid leukemia (AML) [6], chronic lymphocytic leukemia (CLL) [7] and chronic myeloid leukemia (CML) [8]. Acute ones manifest rapidly and necessitate prompt medical attention, but chronic ones take their time to manifest and may initially show no symptoms at all [9]. Given the heterogeneity in clinical presentation and genetic abnormalities across these subtypes, early detection and accurate classification are critical for initiating appropriate treatment and improving survival outcomes [10].

Traditional detection methods include peripheral blood smear analysis, bone marrow

biopsy, immune-phenotyping, and cytogenetic testing [11]. However, there is a lot of inter-observer variability, and many of these methods are laborious and necessitate specialist knowledge. To overcome these limitations, recent advancements have focused on the integration of automated diagnostic systems and computational models.

The use of artificial intelligence (AI) has the potential to greatly enhance the precision and efficiency of leukemia detection and categorization, making it a game-changer in medical diagnostics [12]. By leveraging large volumes of clinical data, AI-driven models can learn complex patterns in blood smear images, genetic profiles, and laboratory test results that may not be easily discernible by human experts [13]. ML techniques have been applied to various types of input data, including hematological parameters, gene expression profiles and microscopic images of blood cells, to assist in diagnosis and subtype classification [14]. However, traditional ML models, such as Support Vector Machines (SVM), Decision Trees (DT), Random Forests (RF) and k-Nearest Neighbors (k-NN) require handcrafted feature extraction, which limits their scalability and generalization to unseen data.

As a subset of ML, Deep Learning (DL) has grown in popularity as a solution to these problems because of its capacity to automatically generate hierarchical structures from unstructured data [15]. DL models excel at processing very small pictures, such as blood smears, and have demonstrated outstanding performance in image-based leukemia diagnosis workloads [16].Also, DL models can capture spatial hierarchies, textures and morphological variations between healthy and leukemic cells [17]. Recent studies have demonstrated that DL-based models can achieve diagnostic accuracies, and facilitate rapid screening, particularly in under-resourced healthcare settings.

Manescu et al., [18] employed a Multiple Instance Learning for Leukocyte Identification (MILLIE) framework to detect acute leukemia and differentiate between Acute Promyelocytic Leukemia (APL) and other subtypes, even without detailed cell-level annotations. DenseNet121, ResNet50, and MobileNet models have also been evaluated on acute leukemia datasets, achieving superior classification accuracies ranging from after WBC segmentation using active contour methods [19]. A progressive Residual Neural Network with multigranularity (PMG) training framework was used to analyze 21,208 annotated peripheral blood cell images across eight leukemic and five benign cell types. The model demonstrated strong APL detection with high precision [20]. In another study, ALNet leveraged VGG16, ResNet101, DenseNet121, and SENet154 in fine-tuned pipelines with 16,450 single-cell images, achieving high diagnostic accuracy for acute leukemia classification [21].

These models highlight a growing trend toward hybrid architectures, and scalable pipelines tailored for robust leukemia screening and classification. However, most of the aforementioned DL approaches primarily focus on classification tasks after pre-segmenting the white blood cells (WBCs), often requiring separate detection or segmentation stages that can introduce bottlenecks in fully automated diagnostic pipelines. To address these limitations and enable end-to-end leukemia detection from whole blood smear images, object detection models such as You Only Look Once (YOLO) have gained attention. YOLO models are ideal for real-time medical applications due to their lightning-fast localization and object classification capabilities, which allow them to process numerous images in a single forward pass. Unlike traditional convolutional neural network (CNN) based classifiers that rely on cropped and pre-labeled inputs, YOLO can process raw microscopic images and directly detect leukemic cells, thus reducing the need for manual pre-processing. or patch-wise analysis. This streamlines the diagnostic workflow and facilitates large-scale deployment in clinical settings, particularly where expert resources are scarce.

One notable application of YOLO in leukemia detection was presented by Prakash et al., [22] who developed a lightweight and optimized YOLOv8-based architecture tailored for blood smear analysis. Their approach tackled common challenges in medical image classification, such as overfitting and computational inefficiency, by incorporating DWSCNN and a RCBAM into the YOLOv8 framework. These modifications enhanced the model capability to extract discriminative structures whereas significantly reducing the number of parameters. However, although RCBAM is designed to highlight important features, it may sometimes assign high attention weights to redundant or irrelevant regions, which can negatively impact the model's performance.

1.1 Major contributions

To address the above challenge, this study proposes an advanced attention framework called YPALDCdriven by Explainable AI (XAI). Specifically, a novel Pixel-Level Fourth-Order Entropy Guided Class Activation Map (PLFOCAM) is introduced in this model to enhance the interpretability and effectiveness of attention. Unlike conventional CAMs that depend on gradient-based

weighting, which can be unstable or less reliable, the proposed method leverages fourth-order entropy to assign more informative and discriminative weights to feature maps. This entropy-driven approach captures richer contextual cues at the pixel level, enabling the model to focus more accurately on disease-relevant regions in leukemia images. This study is structured as follows: A comprehensive analysis of recent DL procedures for leukemia detection was present in section 2. The proposed methodology of the research was described in section 3. The experimental results and comparative studies are reported in section 4. Finally, Conclusion and future enhancement discussed in section 5.

II. LITERATURE SURVEY

Asar and Ragab [23] developed an optimization algorithm called FOADCNN-LDC that uses an advanced convolutional neural network for the diagnosis and categorization of leukemia. It used the ShuffleNetv2 model for feature extraction and CDAE model to perform the detection and classification tasks. To enhance the performance of the CDAE model, the hyper parameters were fine-tuned using the Falcon Optimization Algorithm (FOA). However, the model may hinder real-time or embedded deployment unless optimized which may cause lower accuracy. Awad & Aly [24] created a technique for detecting ALL using the YOLOv8 and YOLOv11 DL models. Initially, the blood smear images were preprocessed to remove irrelevant elements such as background noise and unrelated blood components. Data augmentation methods such as mosaic augmentation and random rotation were used to increase robustness and avoid overfitting. Then, both the YOLOv8 and YOLOv11s model were selected for evaluation. However, the specificity of the model was compromised due to an imbalanced dataset, which marginally affected the model's capacity to accurately categorize normal cells.

Awais et al. [25] developed a way to sort ALL into two groups and subtypes. Initially, they used a Greedy Differential Evolution (GDE) method to strengthen the visual contrast. This method used local neighborhood pixel values to better preserve edges and improve contrast adaptively. However, training used fixed parameters which may not be optimal across all datasets, thereby affects accuracy values. Himel et al. [26] developed a dual-phase ensemble DL-based Computer Aided Diagnosis model to diagnose acute leukemia by analyzing blood smear images under a microscope. The model uses two stages: augmented images using rotation and flipping, and image enhancement techniques. The model extracts feature maps from the last dense layers of two base models, which are then sent to a fully linked meta-classifier for classification. However, the ensemble structure increases memory usage during deployment.

Mahesh et al. [27] introduced a hybrid optimization technique combining to improve feature selection for leukemia prediction using microarray gene expression data when used with Particle Swarm Optimization(PSO), Ant Lion Optimizer (ALO). This strategy combines the exploration and exploitation skills of these algorithms to make feature selection more accurate and faster to converge. But, the model relies on fine-tuning multiple parameters, which are time-consuming and sensitive to initial settings. Using microscope images of blood smears, Shree et al. [28] trained an Optimized Deep Recurrent Neural Network (ODRNN) based on deep learning to aid in the diagnosis of leukemia. In order to extract characteristics and categorize them, the approach employed DRNNs. The DRNN's performance was enhanced by optimizing its weights using the Red Deer Optimization Algorithm (RDOA). Due to its great computational complexity, the model, however, displays lower recall and precision.

Almahdawi et al. [29] suggested a DL-based way to use microscope pictures to diagnose leukemia cells by combining Particle Swarm Optimization (PSO) and Ant Colony Optimization (ACO) to indicate one feature at a time. However, small dataset size restricts the generalizability and robustness of the conclusions, limiting confidence in specificity. Dutta et al. [30] created a multi-class classification approach for ALL using peripheral blood smear (PBS) images and an attention-based CNN model called LEU3. But, the model relies heavily on high-quality datasets, which may not always reflect real-world data variability. Thiriveedhi et al. [31] presented a modified CNN named ALL-Net to distinguish between benign (hematogones) and malignant (Early-B, Pre-B, and Pro-B) cells based on the PBS images of the latter. However,the performance then can break down when trained/deployed on poor-quality data or datasets.

III. PROPOSED METHODOLOGY

In this section, the given methodology is completely illustrated. Fig. 1 depicts the schematic representation of the suggested technique.

3.1 Image Pre-processing

Effective pre-processing greatly affects the efficiency of object detection models in medical image analysis, particularly for hematological malignancies, by increasing clarity and consistency across different samples. In this study, a hybrid pre-processing approach was adopted to enhance blood cell images for efficient leukemia detection.

- Initially, an edge-preserving bilateral filter [32] was applied to remove background noise while maintaining the sharp boundaries of white blood cells, ensuring the retention of morphological details critical for classification.
- Then, Color Deconvolution [33] is applied to separate overlapping stain components. In this context, it helped isolate nucleus-rich regions by separating eosin and hematoxylin stain components, thereby enhancing contrast between leukemic and non-leukemic cells.
- Further, adaptive histogram equalization method [34] was applied to the stain-separated channels to enhance cellular structures and improve local contrast without causing overexposure. Also, this method adjusts image intensity based on local regions, making it more effective for images with uneven lighting.
- Z-score normalization [35] was applied to scale pixel intensities to a standardized range, improving feature consistency for the YOLOv8 detection pipeline.

This pre-processing pipeline ensures the fine-grained details critical for distinguishing between malignant and benign cells are preserved and emphasized. The result is improved detection accuracy, especially in early-stage leukemia where visual differences are often subtle and localized.

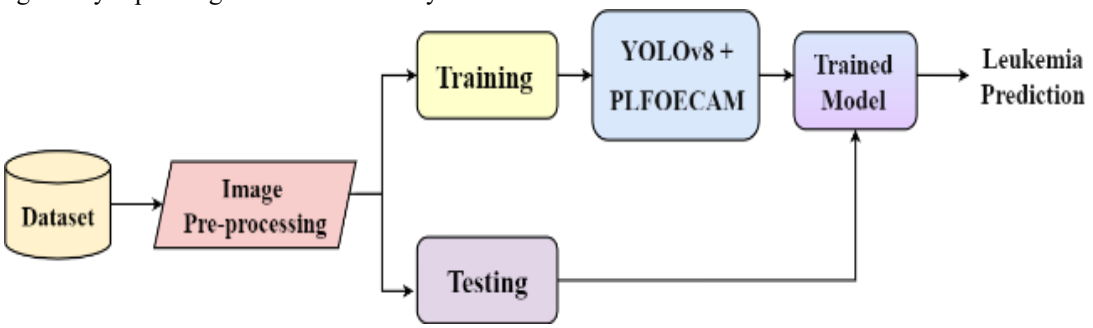

Figure 1. Overall flow of the suggested technique

This pre-processing pipeline ensures the fine-grained details critical for distinguishing between malignant and benign cells are preserved and emphasized. The result is improved detection accuracy, especially in early-stage leukemia where visual differences are often subtle and localized.

3.2 General YoloV8 Structure

YOLOv8 is applied for real-time object detection and image segmentation model developed by Ultralytics. It features an anchor-free architecture, improved feature extraction and high adaptability across various model sizes (nano to extra-large). YOLOv8 is perfect for real-world detection and medical applications because it strikes a great balance between speed and accuracy. The three primary parts that make up YOLOv8's architecture are the backbone, the neck, and the head.

The **Backbone** based on Cross Stage Partial Darknet-53 (CSPDarknet53), is responsible for feature extraction. It uses standard convolutional (Conv) layers to produce initial feature maps and Cross Stage Partial (C2f) layers to improve gradient flow and learning efficiency. Within the C2f module, bottleneck blocks are employed to compress and refine the feature maps, reducing redundancy while maintaining essential information for the subsequent stages.

The **Neck** connects the spinal column to the brain by fusing features at different scales. It takes its design cues from PANet and the Feature Pyramid Network (FPN). This component enhances

information flow and aggregates features using both top-down and bottom-up pathways, effectively preserving fine-grained spatial details and improving detection at multiple scales.

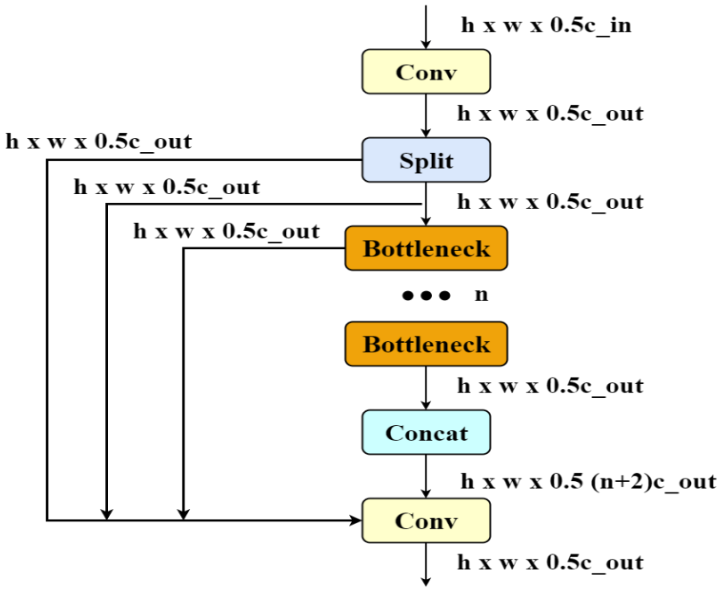

Figure 2.(a) C2f Structure

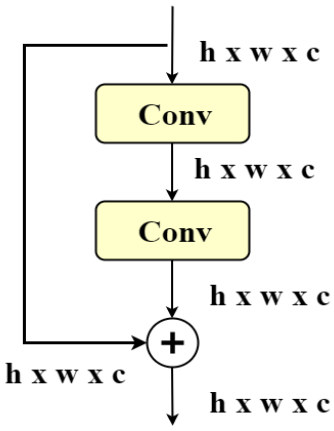

Figure 2. (b) bottleneck

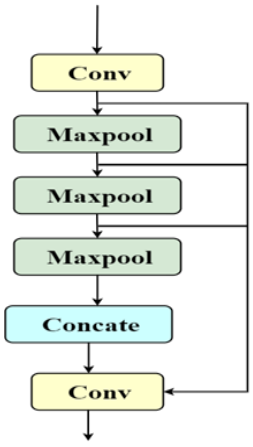

Figure 2. (c) SPFF module

The **Head** component generates the final predictions for object detection, which include confidence scores, class probabilities, and bounding box coordinates. It utilizes convolutional layers to refine features passed from the neck and supports loss computation during training. The head transforms high-level visual features into actionable detection data, ensuring accurate localization and classification across various object sizes.

Since, the standard YOLOv8 lacks the fine-grained feature extraction needed for subtle leukemia detection, the authors enhanced it by integrating DWSCNN and RCBAM. These additions improved accuracy and contextual focus while reducing model complexity. As a result, the modified YOLOv8 achieved faster inference speed highly suitable for real-time clinical use.

Since the standard YOLOv8 architecture lacks the fine-grained feature extraction required for detecting subtle patterns in leukemia, the authors enhanced it by incorporating DWSCNN and RCBAM. These enhancements improved both

contextual focus and detection accuracy while reducing model complexity. As a result, the tweaked YOLOv8 has better performance and faster inference speed, making it ideal for use in real-time clinical settings.

3.3 Enhanced YOLOV8 Structure

The enhanced YOLOv8 structure optimized for leukemia detection is illustrated below. Its modifications improve fine-grained feature extraction and contextual information aggregation, both critical for accurately detecting and staging blood cancer.

3.3.1 Enhanced Backbone

Starting with an input image of dimensions 640 × 640 × 3, the upgraded YOLOv8 model gradually decreases the image's spatial accuracy while increasing the length of the feature channels, forming its backbone. Initially, convolutional (Conv) layers reduce the dimensions from 320 × 320 × 16 to 160 × 160 × 32. A C2f block maintains the size at 160 × 160 × 32, while refining feature representations.

To improve efficiency, the model incorporates DWSCNN layers. DWSCNN used a two-step process like depthwise convolution and pointwise convolution. Fig.3 depicts the DWSCNN Architecture.

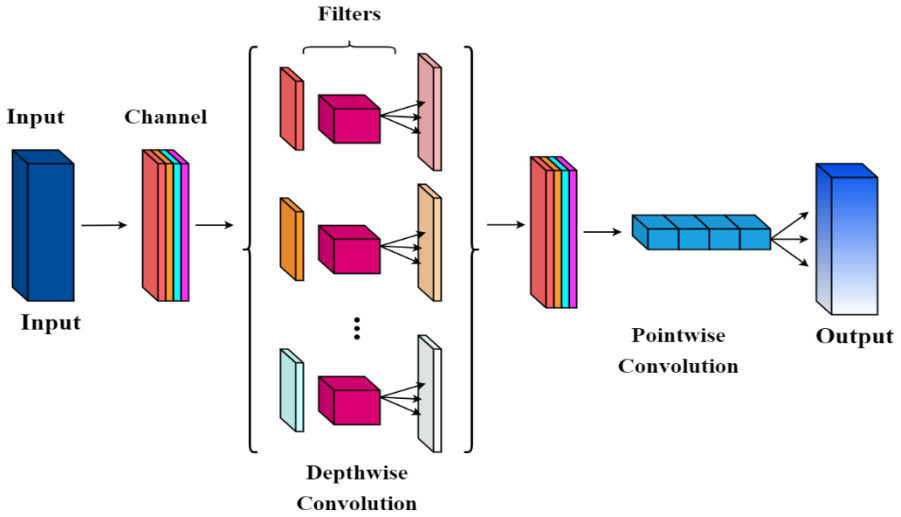

Figure 3. DWSCNN Architecture

After applying a distinct filter to each input channel in depthwise convolution, the outputs are fused using a 1 x 1 kernel in pointwise convolution. This structure significantly reduces computational cost while preserving critical feature information. The downsampling continues until the spatial size reaches 20 × 20 × 256, at which point the data enters the SPPF block. This block combines multi-scale features, enabling robust detection across varying object sizes. The application DWSCNN is particularly advantageous for processing high-resolution blood smear images, as it ensures rapid, accurate feature extraction. Because it keeps computational overhead minimal, the model can be deployed on devices with limited resources and used in real-time applications.

3.3.2 Enhanced Neck

The neck module begins by upsampling the 20 × 20 × 256 feature map to 40 × 40 × 128, which is concatenated with the corresponding feature map from the backbone, forming a 40 × 40 × 256 map. This is refined using a RCBAM and a C2f block maintaining the output size of 40 × 40 × 128. Similar process follows with upsampling to 80 × 80 × 64, concatenation, and refinement using another RCBAM and C2f preserving the 80 × 80 × 64 resolution.

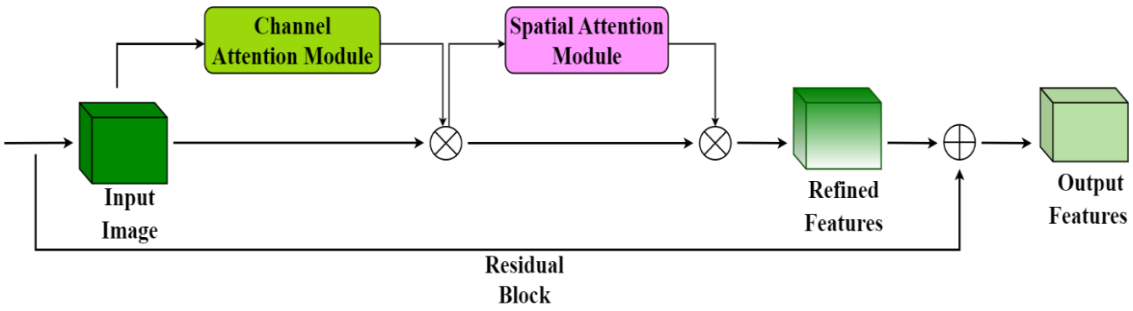

Figure 4. Design of RCBAM

Fig. 4 depicts the structure of RCBAM module. In the bottom-up pathway, convolutional layers reduce the map to 40 × 40 × 128, which is concatenated with earlier features and processed by a C2f block to yield 40 × 40 × 192. Further C2f block made a reduction to 20 × 20 × 256 is performed followed by final concatenation with backbone features and processing through RCBAM and a concluding C2f block.

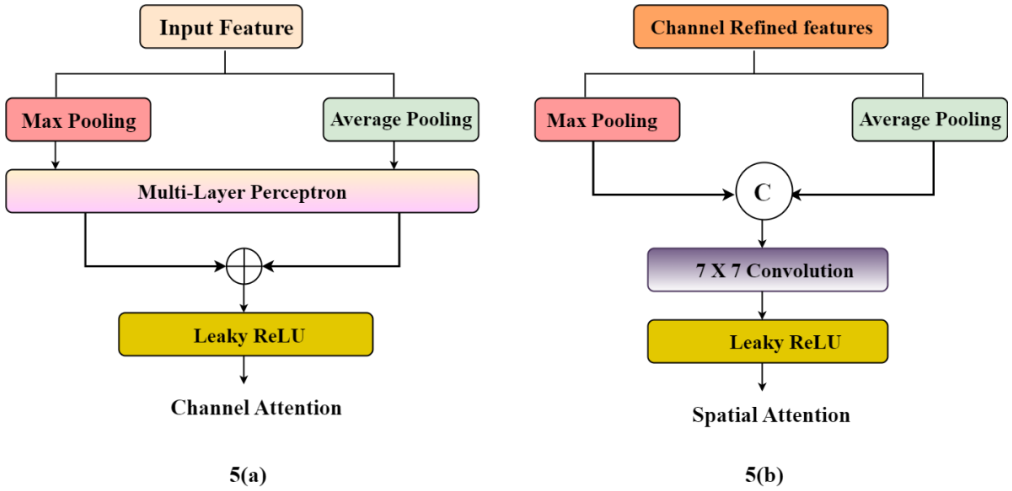

Figure 5. (a) Channel Attention 5(b) Spatial Attention

The RCBAM block improves significant functionalities through two attention: channel attention and spatial attention. Channel attention applies average (F_{avg}^{C}) and maximum (F_{max}^{C}) pooling, followed by a common Multi-Layer Perceptron (MLP) is generating an attention map as in equation (1)

$$M_c(F) = \sigma\left(MLP\left(Avgpool(F)\right) + MLP\left(Maxpool(F)\right)\right) = \sigma\left(W_1\left(W_0 F_{avg}^{C}\right)\right) + \left(W_1\left(W_0 F_{max}^{C}\right)\right) \quad (1)$$

Where, $M_c(F)$ is the channel attention map obtained from the feature map F. σ is the sigmoid activation map, W_0 and W_1 are the MLP weights, F_{avg}^{C} and F_{max}^{C} are the average and max-pooled features on the channel dimensions. Afterwards, the channel-weighted feature map that is produced is fine-tuned by employing spatial attention, which brings together spatial data by average and max pooling, and then a 7×7 convolution, just like in equation (2).

$$M_c(F) = \sigma\left(f^{7\times7}([Avgpool(F); Maxpool(F);])\right) \quad (2)$$

Where, the convolution operation $f^{7\times7}$ has a filter size of 7×7.

In order for RCBAM to function properly, it combines channel attention with spatial attention. The channel attention module and the spatial attention

module's respective structures are shown in Fig. 5(a) and 5(b).

To get F', apply channel attention to the feature map F as in equation (3)

$$F' = M_c(F) \otimes F \tag{3}$$

To get F'', apply channel attention to the feature map F' as in equation (4)

$$F'' = M_s(F') \otimes F' \tag{4}$$

These residual attention enhancements help preserve key features, improve focus on informative regions, and support robust feature learning essential for accurate leukemia detection.

3.3.3 Enhanced Head

The Head section of the network is designed for multi-scale object detection. It processes the 80 × 80 × 64, 40 × 40 × 128 and 20 × 20 × 256 feature maps from the Neck through separate detection blocks each optimized for identifying large, medium and small objects respectively. This multi-scale approach uses the improved features from the Backbone and Neck to accurately detect blood cancer cells of different sizes and stages. Every Detect layer manages different spatial resolutions, allowing for fine-grained detection and classification crucial for accurate blood cancer staging.

The integration of DWSCNN and RCBAM layers significantly enhances the YOLOv8 architecture. DWSCNN layers reduce computational complexity while preserving fine feature details and crucial for identifying subtle differences in blood cancer cells. Enhancing the model's capacity to differentiate between blood cancer stages, RCBAM layers incorporate attention methods that allow it to zero in on the most informative areas of the feature maps. This combination effectively handles the complex and varied presentation of blood cancer for better decision-making.

3.4 Design of PLFOECAM

Explainable AI (XAI) is vital in medical imaging as it enhances the transparency and interpretability of deep learning models. For critical tasks like leukemia detection, it ensures not only high accuracy but also clear visual explanations of model decisions. Traditional DL models often act as "black boxes," lacking insight into their predictions. XAI techniques, like CAMs, aid in identifying critical areas in input photos; however, conventional CAMs often rely on gradients, which can be unstable or noisy.

To address the limitations of gradient-based CAMs, this study introduces a novel attention mechanism called PLFOECAM. Instead of relying on gradients, PLFOECAM uses pixel-level fourth-order entropy to weight feature maps, enhancing the stability and interpretability of attention maps. This entropy-driven approach highlights regions with high informational complexity, capturing richer contextual cues. Integrated into the YOLOv8 pipeline, PLFOECAM enables more reliable focus on subtle, clinically relevant features in leukemia detection.

Consider the scalar conservation law in the feature space as in equation (5)

$$\frac{\partial}{\partial t}a + \frac{\partial}{\partial x}f(u) = 0 \tag{5}$$

Where, u is the deep feature map value at pixel level, $f(u)$ will be the spatial distribution entropy in CAM. a can be interpreted as entropy accumulation over time (e.g., over layers or frames). The entropy solution satisfies the entropy condition for CAM stability as given in equation (6)

$$\frac{\partial}{\partial t}\eta(u) + \frac{\partial}{\partial t}q(u) \leq 0 \tag{6}$$

Here, $\eta(u) = E^4(x, y)$ will be the fourth order entropy function of feature map u. $q(u)$ is the entropy flux i.e., movement of information saliency in CAM. Also, it satisfies the entropy variable $\gamma = \frac{\partial \eta}{\partial u}$. The semi-discrete strategy, as in equation (7), is used to answer equation (5) using the conservative difference method.

$$\frac{du_i}{dt} = \frac{f_{i+1/2} - f_{i-1/2}}{\Delta x} \tag{7}$$

Where, u_i represents the pixel-level activation at the uniform node x_i Geometric grid. $f_{i+1/2}$ and $f_{i-1/2}$ will be difference between the entropy between adjacent pixels. If equation (7) meets a discrete form of the entropy criterion as in equation (6), updated in equation (8), we say that it is entropy stable.

$$\frac{\partial}{\partial t}\eta(u_i) + \frac{q_{i+1/2} - q_{i-1/2}}{\Delta x} \leq 0 \quad (8)$$

$\eta(u_i)$ is the fourth order entropy function of feature map u. This ensures the attention map remains consistent, without artificial amplification. The entropy conservative equation (8) is equivalent to the discrete entropy equality in equation (9) when implemented.

$$\frac{\partial}{\partial t}\eta(u_i) + \frac{q_{i+1/2} - q_{i-1/2}}{\Delta x} = 0 \quad (9)$$

In this work, the ordinary equation (7) is solved using a four-order Runge-kutta technique. Improving the numerical flow $f_{i+1/2}$ that is entropy stable is the current emphasis. The numerical flux is first divided into two parts, one for entropy conservatism and the other for numerical diffusion, based on equation (10)

$$f_{i+1/2} = f^{EC}_{i+1/2} - \frac{1}{2}\,\delta_{i+1/2}\left(v^{+}_{i+1/2} - v^{1}_{i+1/2}\right) \quad (10)$$

Where, $f^{EC}_{i+1/2}$ is the conservative CAM flow, $\delta_{i+1/2}$ is the entropy based attention weight, $v^{+}_{i+1/2}$ is the CAM attention values reconstructed on the pixel interface, equation (10) constructs the CAM maps using the fourth–order entropy reconstruction.
Here, $f^{EC}_{i+1/2}$ is the fourth order entropy conservative flux is expressed in equation (11)

$$f^{EC}_{i+1/2} = \frac{4}{3}\hat{f}\,(u_i, u_{i+1}) - \frac{1}{6}\hat{f}\,(u_{i-1}, u_{i+1}) - \hat{f}\,(u_i, u_{i+2}) \quad (11)$$

Tadmor [36] defines the second-order entropy conservative flow as$\hat{f}\,(\alpha, \beta)$, which represents the pairwise entropy similarity between feature pixels. This ensures smooth yet accurate propagation of attention information.In most cases, the value of $\delta_{i+1/2}$ in the numerical diffusion section is selected as $\left[f'\left(u_{i+1/2}\right)\right]$. If the entropy variables v_i reconstrued values at the interfaces $v^{+}_{i+1/2}$ satisfy equation (12)

$$sign\left(v^{+}_{i+1/2} - v^{1}_{i+1/2}\right) = sign\,(v_{i+1} - v_i) \quad (12)$$

The numerical flux in equation (11) achieves entropy stability for PLFOECAM. When the sign of the underlying point value leap matches the sign of the reconstructed point values at each cell interface, then equation (12) satisfies the sign property. This is crucial in PLFOECAM to ensure entropy-weighted attention aligns with local intensity transitions. The fourth order reconstruction is provided in order to meet the sign property as follows to get $v^{+}_{i+1/2}$. Take the polynomial reconstruction in equation (13)

$$p_i\,(x) = v_i + d_i\left(\frac{x - x_i}{\Delta x}\right) + \left(\frac{v_{i-1} - 2v_i + v_{i+1}}{2}\right)\left(\frac{x - x_i}{\Delta x}\right)^2 + \left(\frac{-v_{i-1} + v_{i+1} - 2d_i}{2}\right)\left(\frac{x - x_i}{\Delta x}\right)^3 \quad (13)$$

Where, $p_i\,(x)$ is the smooth reconstruction of entropy based CAM. d_i being the slope function of entropy variation around pixel i. This yields a fourth-order smooth PLFOECAM map that reduces noise and sharpens attention on key pathological features in leukemic cells.

3.5 Integrating PLFOECAM in YOLOv8

In the proposed YOLOv8 architecture for leukemia detection, the PLFOECAM module is integrated into three different scales within the head section to enhance visual interpretability through explainable AI. Specifically, PLFOECAM is applied after the detect heads responsible for predicting class probabilities at three spatial resolutions: 80 × 80 × 64 × w, 40 × 40 × 128 × w, and 20 × 20 × 256 × w × r. At each of these levels, once the class predictions are computed by the detect layer, PLFOECAM utilizes the corresponding feature maps to generate pixel-level fourth-order entropy guided class activation maps that highlight regions with high informational complexity, such as leukemic nuclei and abnormal morphological structures, while suppressing less relevant or redundant area. Fig. 6 represents the integration of PLFOECAM in YOLOv8.

To compute this attention, the feature maps $F_k(x, y)$ from the detect head are first normalized across channels to determine the soft activations as in equation (14)

$$p_k(x, y) = \frac{F_k(x,y)}{\sum_{j=1}^{K} F_j(x,y) + \epsilon} \quad (14)$$

Using these normalized activations, the pixel-wise fourth order entropy is calculated as in equation (15)

$$E^4(x, y) = -\sum_{k=1}^{K} p_k(x, y)^4 . log(p_k(x, y)^4 + \epsilon)$$

(15)

This entropy map quantifies the information richness at each pixel. Then, channel-wise attention weights are derived by combining entropy with original activations as in equation (16)

$$a_k = \frac{1}{Z} \sum_{x=1}^{H} \sum_{y=1}^{W} E^4(x,y).F_k(x,y) \quad (16)$$

The resulting PLFOECAM attention map is computed by applying these weights over the original feature channels as in equation (17)

$$PLFOECAM\ (x,y) = ReLU\left(\sum_{k=1}^{K} a_k.F_k(x,y)\right) \quad (17)$$

This map is then up-sampled to match the resolution of the preceding layers in the architecture and injected back into earlier stages. The up-sampled attention output from the 20 × 20 × 256 × w × r level is fused into the neck section just before the C2f layer. Similarly, the output from the 40 × 40 × 128 × w scale is fed into the neck before the convolutional fusion and RCBAM block, while the attention map from the 80 × 80 × 64 × w scale is injected into the backbone before the corresponding convolutional block. The fusion of PLFOECAM into the feature hierarchy is mathematically modelled as in equation (18)

$$F_k^{fused}(x,y) = F_k^{pre}(x,y) + \lambda.A^{up}\ (x,y) \quad (18)$$

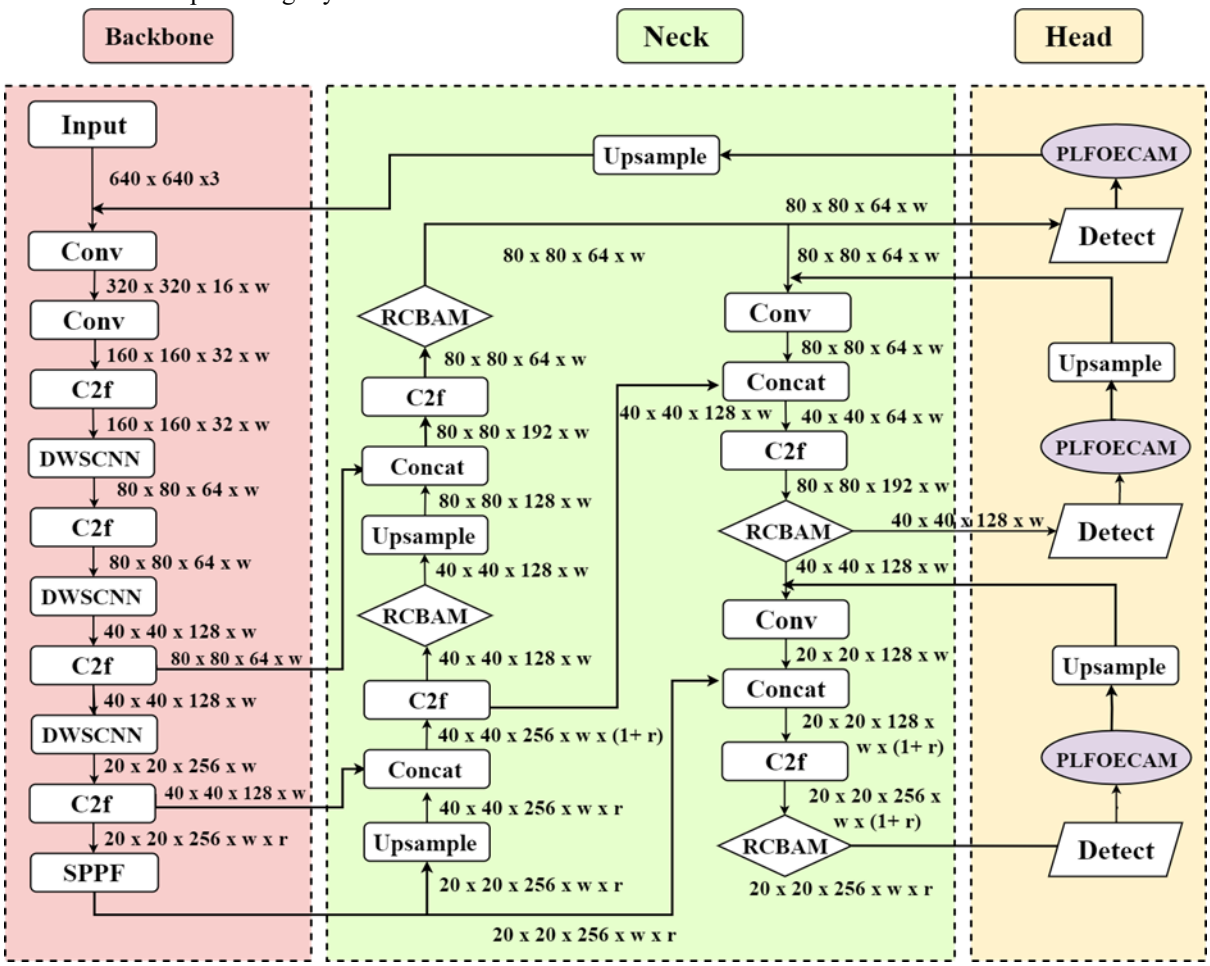

Figure 6. Block Structure of the Proposed PLFOECAM in YOLOv8 Model (* w = width; r = ratio)

Where, $F_k^{fused}(x,y)$ the original feature map before convolution, $A^{up}\ (x,y)$ is the upsampled PLFOECAM attention map and λ is a scaling factor controlling attention influence. This feedback mechanism allows high-level semantic attention to guide and refine low- and mid-level feature learning

across both the backbone and neck. As a result, the proposed architecture enhances spatial awareness, improves focus on diagnostic features and offers better explainability and confidence for automated leukemia detection.

3.6 Detection and Classification

In the proposed PLFOECAM-enhanced YOLOv8 architecture for leukemia detection, the detect head plays a central role in producing both the bounding box predictions and the class probabilities required to localize and identify leukemic cells. Fig. 7 depicts the Detect Head's Structure.

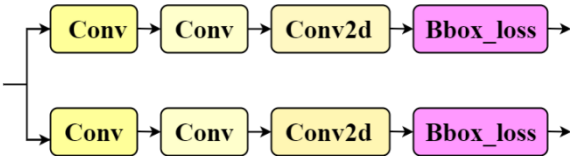

Figure 7. Detect Head's Structure

As illustrated, each detect head consists of multiple convolutional layers that separately handle object localization and classification. Specifically, at each scale (20×20, 40×40, and 80×80), the feature maps from the neck are first processed through stacked convolutional blocks to generate intermediate spatial representations. These are then passed through final Conv2D layers to compute the bounding box regression output and the classification logits.The bounding box regression module predicts four coordinates (x, y, w, h) for each detected region, optimized using a loss such as Complete Intersection of Union (cIoU) as in equation (19)

$$\mathcal{L}_{bbox} = 1 - \text{cIoU}\left(bb_p, bb_{gt}\right) \quad (19)$$

Where the predicted bounding box is denoted as bb_p and the ground truth bounding box as bb_{gt}. Simultaneously, the classification head produces a set of logits for each class, which are converted to probabilities via the softmax function as in equation (20)

$$P(c_i|x, y) = \frac{e^{z_i}}{\sum_{j=1}^{C} e^{z_j}} \quad (20)$$

Where, $P\ (c_i)$ suppresses the final class probability for class i, C is the total number of leukemia subtypes and z_i is the logit for class i. According to equation (21), the classification loss is calculated by taking the cross entropy of the predicted probability and the ground truth class labels.

$$L_{cls} = \sum_{i=1}^{C} y_i \,.\, log\big(P(c_i)\big) \quad (21)$$

The total detection loss is a combination of both localization and classification elements as in equation (22)

$$L_{total} = \lambda_{bb} \,.\, L_{bb} + \lambda_{cls} \,.\, L_{cls} \quad (22)$$

Where, the weighting factors that equalize the impact of each loss term are denoted as λ_{bb} and λ_{cls}. Following the location of the bounding boxes and the results of the class's confidence tests are predicted at each detection scale, these outputs are passed to the PLFOECAM module to generate entropy-guided class activation maps. The leukemia detection process is made easier to understand with the help of these maps, which show the specific geographic areas that the model used to make its predictions. The integration of PLFOECAM ensures that even subtle leukemic cell patterns are effectively captured and visualized providing more transparent decision-making task through entropy-based attention heatmaps for accurate leukemia prediction.

Algorithm: YPALDC for Leukemia Detection and Classification

Input: Blood smear image from leukemia dataset

Output: Leukemia prediction

1. Start
2. **Image Preprocessing**
3. Apply bilateral filter to remove background noise while preserving WBC boundaries
4. Perform color deconvolution to separate eosin and hematoxylin stain components
5. Enhance contrast via adaptive histogram equalization
6. Normalize pixel intensity using Z-score normalization
7. **Feature Extraction – Enhanced YOLOv8 Backbone**
8. Resize image to 640×640×3 pass through initial convolutional layers
9. Apply DWSCNN for lightweight feature extraction
10. Pass through C2f blocks and SPPF for multiscale contextual learning

11. Extract multi-resolution features at scales 20×20, 40×40, 80×80
12. **\\Context Aggregation – Enhanced Neck**
13. Perform upsampling and concatenation for multi-scale fusion
14. Apply RCBAM
15. Compute channel attention via pooled MLP layers (equation 1)
16. Compute spatial attention via 7×7 convolution (equation 2)
17. Refine features using C2f blocks at each scale
18. **\\PLFOECAM**
19. Extract feature maps from each detection head
20. Normalize activations across channels (equation 14)
21. Compute fourth-order entropy map at each pixel (equation 15)
22. Calculate entropy-based channel attention weights (equation 16)
23. Generate PLFOECAM attention maps by weighted sum of channels (equation 17)
24. Upsample attention maps to match resolution and inject into Backbone, Neck and Head of YOLOv8
25. Fuse attention maps with original features using residual connection (equation 18)
26. **\\Detect Head**
27. Predict bounding boxes and class scores at 3 scales (small, medium, large objects)
28. Compute bounding box loss using Complete IoU (equation 19)
29. Compute class probabilities using softmax (equation 20)
30. Compute classification loss using cross-entropy (equation 21)
31. **\\Final Prediction and Visualization**
32. Refine detection output with entropy-enhanced features
33. Generate final bounding boxes and leukemia subtype classification
34. Produce interpretable heatmaps highlighting key regions via PLFOECAM
35. End

Thus, the proposed YPALDC model effectively enhances leukemia detection and classification by integrating PLFOECAM into the YOLOv8 framework, enabling accurate predictions with improved interpretability and diagnostic confidence.

IV. RESULT AND DISCUSSION

a. Data Description

There are three datasets that have been used for the experiments.

SN-AM Dataset [37]: The Nikon Eclipse-200 microscope was used to acquire images at a resolution of 1000x from bone marrow aspirate slides of individuals who were diagnosed with B-lineage ALL (B-ALL) and with MM. Staining the slides with Jenner-Giemsa was done. Ninety B-ALL photos and one hundred MM images totaling 2560x1920 pixels were taken in raw BMP format. There is enough variation in MM and B-ALL pictures from one image to the next to allow for a thorough testing of any suggested stain normalization techniques.

MiMM_SBILab Dataset [38]: The images were captured at a magnification of 1000x using a digital camera and a Nikon Eclipse-200 microscope. The bone marrow aspirate slides of individuals with multiple myeloma (MM) were stained with Jenner-Giemsa stain. The 85 photos are all stored in raw BMP format and have dimensions of 2560 by 1920 pixels. Our patented technology was used to stain normalize all 85 photos, ensuring that they are adequate for cell segmentation tasks.

C-NMC dataset [39]: The ALL Disease Diagnostics Competition was an opportunity for the Cancer Imaging Archive (TCIA) to make this dataset available. It covers 10,661 micrographs of blood clots, divided as follows: 7272 from 47 leukemia patients and 3389 from 26 healthy people. The photographs are 450 by 450 pixels in size and use a 24-bit RGB color format.

b. Experimental Evaluation and Performance metrices

Using the dataset provided in section 4.1, this section compares the proposed YPALDC model to other existing models. The code was executed in Python 3.11 on a PC with an Intel CoreTM.i5-4210 3GHz, 4GB RAM, and 1TB HDD running Windows 10 64-bit. One option is to use all of the data with 4-fold cross validation, while another is to split the data into 70% training and 30% testing. The model's confusion matrix, as shown in Table 1, when applied to the test data set. Table 2 depicts the parameter settings for the proposed work.

Table 1. Confusion Matrix for Proposed and Existing Models on Testing Set

Dataset	Class	TP	TN	FP	FN
SN-AM Dataset	ALL	84	169	7	10
	AML	85	170	6	9
	MM	84	169	7	10
MiMM_ SBILab	MM	440	414	6	20
	Non-MM	414	440	6	20
C-NMC dataset	ALL	1370	1370	122	140
	Normal	980	1370	122	140

The model's ability to forecast MI from the available datasets is assessed using the following performance measures.

Intersection over Union (IoU): It evaluates the degree to which the leukemia region annotations on the ground and the anticipated PLFOECAM heatmap overlap. Like in equation (23) it quantifies the accuracy with which the predicted region pinpoints the real leukemic regions.

Table 2. Hyperparameter Settings for YPALDC Model

Hyperparameter	**Value**
Batch Size	32
Number of Epochs	100
Learning Rate	0.001
Optimizer	Adam
Dropout Rate	0.5
PLFOECAM Entropy Scaling Factor (α)	0.5 – 1.0
PLFOECAM Solver	Runge-Kutta (Order 4)
Activation Function	ReLU
Input Image Size	640 × 640
Normalization Method	Z-score
Detection Scales	80×80, 40×40, 20×20
Channel MLP Ratio	1/2
CBAM Spatial Kernel Size	7 × 7

$$IoU = \frac{|Heatmap \cap Groundtruth|}{|Heatmap \cup Groundtruth|} \quad (23)$$

Dice Coefficient (DC): Using recall and precision, the DC determines how close the predicted region is to the ground reality. According to equation (24), it works very well for segmenting and localizing different sized regions in medical images:

$$DC = \frac{2\times|Heatmap \cap Groundtruth|}{|Heatmap|+|Groundtruth|} \quad (24)$$

Accuracy: According to equation (25), it is calculated as the ratio of the number of samples to the proportion of cases that were correctly identified (both leukemia and non-leukemia):

$$Accuracy = \frac{TP+TN}{TP+TN+FP+FN} \quad (25)$$

In equation (26), True Positive (TP) means that the model correctly predicted a leukemia case. When the model correctly identifies a case that is not leukemia, it is called a true negative (TN). False Positive (FP) denotes non-leukemia case incorrectly classified as leukemia. False Negative (FN) refers where leukemia cases incorrectly classified as non-leukemia cases.

Precision: The model's accuracy in predicting leukemia cases is determined by dividing all positive predictions by the total number of cases, as shown in equation (26)

$$Precision = \frac{TP}{TP+FP} \quad (26)$$

Recall\Sensitivity: The percentage of true leukemia cases that the model accurately identified is computed using the formula in equation (27)

$$Recall = \frac{TP}{TP+FN} \quad (27)$$

F1-score: In equation (28) shows that it is the weighted mean of recall and precision.

$$F1-score = \frac{2\times Precision\times Recall}{Precision+Recall} \quad (28)$$

c. Performance Evaluation of Different CAM models

In this section, the proposed PLFOECAM model is compared with standard visualization models like CAM, Grad-CAM, Grad-CAM++ and Layer CAM. These models are evaluated using different metrics like IoU and DC as in section 4.2 The illustration of these standard visualization models is given below.

CAM: By superimposing the final classification layer's weights onto the convolutional feature maps, CAM employs global average pooling to produce attention maps that are class-specific. Although simple and interpretable, CAM is limited to specific network architectures and tends to offer low spatial resolution, which can hinder precise medical region localization.

Grad-CAM: Grad-CAM takes a look at the target class gradients that go into the final convolutional layer to figure out how important each feature map. It typically produces localization maps that are somewhat coarse, making it difficult to identify important details in leukemia cell images that are either too small or too subtle to be picked up by such maps.

Grad-CAM++: Grad-CAM++ ranges Grad-CAM by combining higher-order derivatives, allowing for improved localization of multiple discriminative regions in a single image. This is especially useful in complex datasets with overlapping structures. However, its performance is still bounded by the quality of backpropagated gradients, which may be noisy in deeper models.

Layer-CAM: Layer-CAM improves spatial detail by leveraging element-wise gradients across different layers, thus enhancing localization precision in shallow and deep parts of the network. It addresses some spatial limitations of Grad-CAM but still retains dependency on gradient flow and lacks a statistical interpretation of pixel importance.

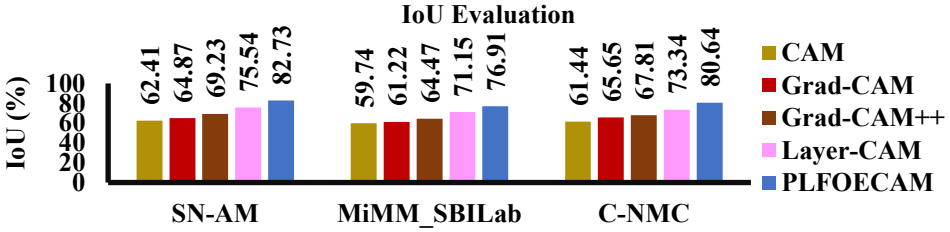

Figure 8. IoU comparison of PLFOECAM with alternative visualization techniques

In Fig. 8 and Fig. 9 depicts the IoU and DC evaluation for three dataset. In this analysis, the proposed PLFOECAM model achieves highest IoU and DC values than other standard models. This consistent improvement highlights PLFOECAM's ability to capture fine-grained leukemic features with greater spatial precision. Its fourth-order entropy mechanism enables better discrimination of pathological regions compared to gradient-based CAMs. The enhanced attention maps lead to more accurate and interpretable localization across diverse staining and cell morphology conditions.

d. Performance evaluation on classification models

In this segment, the productivity of the suggested YPALDC model compared to integration of visualization methods with CNN models like CAM+YOLOv8, Grad-CAM+ YOLOv8, Grad-CAM++ + YOLOv8 and Layer-CAM+YOLOv8. These models are evaluated using the dataset in Section 4.1 on all key metrics available in Section 4.2. Fig. 10 shows the results of comparing the proposed and existing models for ALL, AML, and MM prediction on the SN-AM dataset. In this analysis, the proposed YPALDC model achieves accuracy is 16.69%, 10.72%, 7.24% and 3.98% higher than CAM+YOLOv8, Grad-CAM+ YOLOv8, Grad-CAM++ + YOLOv8 and Layer-CAM+YOLOv8 models respectively.

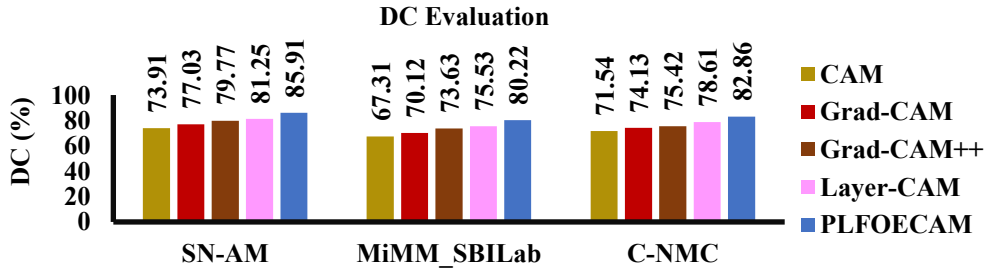

Figure 9. Comparative DC study of alternative visualization approaches to the proposed PLFOECAM

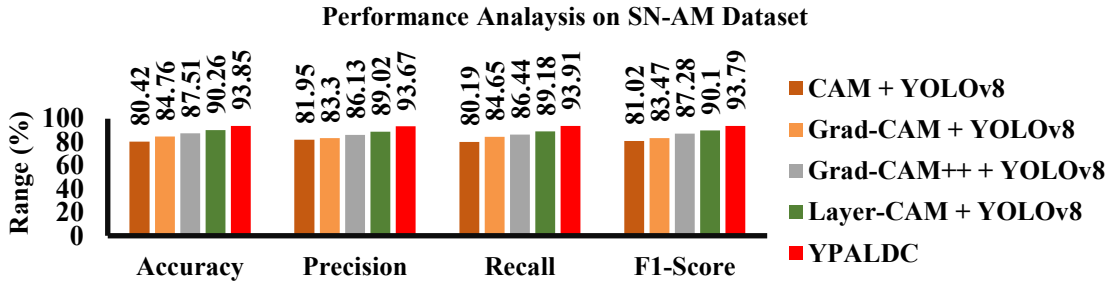

Figure 10. Comparison of Current and Proposed Models for ALL, AML, and MM Prediction Using 4-Fold Cross Validation

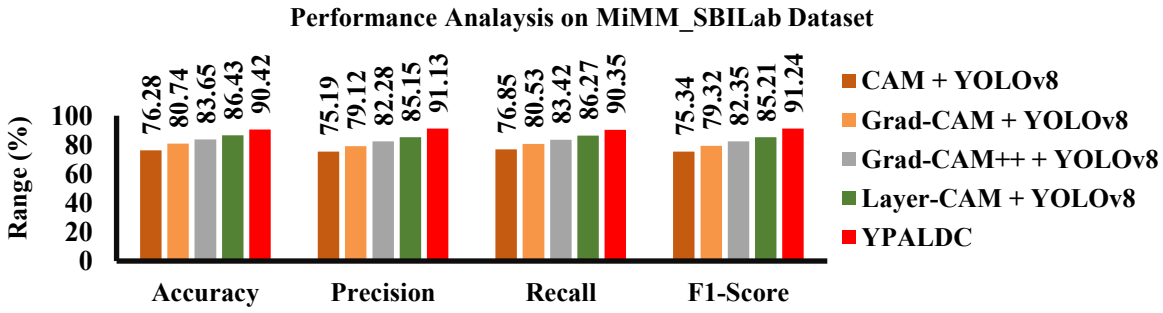

Figure 11. Comparison of Current and Proposed Models for MM Prediction Using 4-Fold Cross Validation

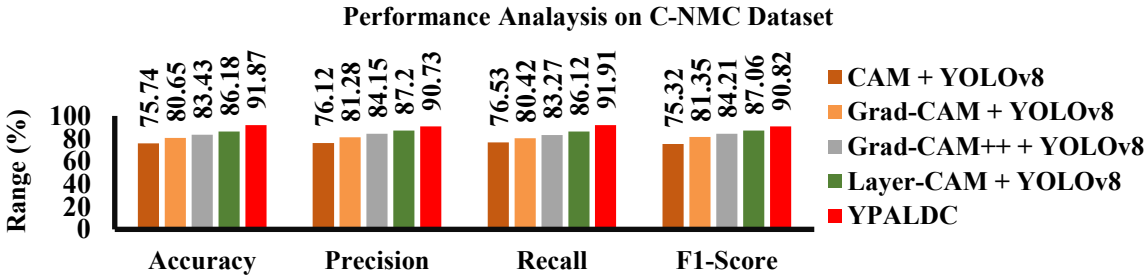

Figure 12. Comparing the Performance of the Proposed and Existing Models for ALL Prediction using 4-fold Cross Validation

Fig. 11 shows the results of comparing the proposed model with the existing one for MM Prediction on the MiMM_SBILab dataset. In this analysis, th proposed YPALDC model achieves accuracy of is 18.54%, 11.98%, 8.09% and 4.61% higher than other models respectively. Similarly, In Fig. 12, we can see the results of comparing the new model with the existing one for ALL prediction on the C-NMC dataset. In this analysis, the proposed YPALDC model achieves accuracy of is 21.29%, 13.91%, 10.12%, 6.6% higher than other models respectively. In this analysis, the proposed YPALDC model provides higher results than other standard models. This is because the proposed YPALDC model effectively integrates the pixel-level entropy-guided attention and optimized feature extraction for accurate leukemia subtype prediction.

Table 3. Comparison of robustness for YPALDC against adversarial inputs

Test condition	**Metrics**	**SN-AM Dataset**	**MiMM_SBILab Dataset**	**C-NMC Dataset**
Without pre-processing (i.e., dataset has	Accuracy (%)	90.13	87.62	88.71
	Precision (%)	89.87	88.30	87.54

adversial input)	Recall (%)	90.35	87.41	88.93
	F1-score (%)	90.10	87.82	88.21
With pre-processing (i.e., dataset has no adversarial inputs)	Accuracy (%)	93.85	90.42	91.87
	Precision (%)	93.67	91.13	90.73
	Recall (%)	93.91	90.35	91.91
	F1-score (%)	93.79	91.24	90.82

Table 3 presents a robustness comparison of the YPALDC model across the SN-AM, MiMM_SBILab, and C-NMC datasets under varying conditions. Without pre-processing, the presence of adversarial noise leads to a clear decline in all key metrics, causing more misclassifications in leukemia subtype prediction. However, applying techniques like normalization and noise reduction significantly improves performance. YPALDC shows greater reliability and consistency in detecting ALL, AML, and MM, even in complex imaging scenarios. This underscores the vital role of pre-processing in enhancing model robustness and generalizability, especially for real-world medical image analysis with noise and background variability.

Table 4 shows the YPALDC model's computational efficiency results on the SN-AM, MiMM_SBILab, and C-NMC datasets simultaneously. Training time, inference time, and memory utilization were measured separately for both CPU and GPU environments. The results clearly indicate that GPU-based training and inference are significantly faster than those on CPU. Among the datasets, SN-AM shows relatively lower computational demands due to its more uniform image quality and structure, while MiMM_SBILab and C-NMC datasets require higher processing power and memory because of greater variability in image quality, background complexity, and class diversity. These factors lead to longer training times and increased memory usage. This underscores the fact that real-world medical datasets are computationally more intensive than clean or standardized ones, and demonstrates the effectiveness of GPU-based implementation in accelerating training and inference while managing memory more efficiently.

Table 4. Computational efficiency of the YPALDC on collected dataset

Computational Metrics		**SN-AM Dataset**	**MiMM_SBILab Dataset**	**C-NMC Dataset**
Training time (sec)	CPU	8120	7635	7890
	GPU	1420	1335	1390
Inference time (sec)	CPU	286	271	278
	GPU	135	123	120
Memory usage (MB)	CPU	6140	5975	6020
	GPU	2140	2035	2080

Table 5. Comparison of YPALDC Model with and without hyperparameter optimization

Test condition	**Metrics**	**SN-AM Dataset**	**MiMM_SBILab Dataset**	**C-NMC Dataset**
Without hyperparameter optimization	Accuracy (%)	89.34	86.52	88.73
	Precision (%)	88.92	87.01	87.56
	Recall (%)	89.45	86.28	88.90
	F1-score (%)	89.18	86.64	88.22
With hyperparameter optimization (Grid search)	Accuracy (%)	93.85	90.42	91.87
	Precision (%)	93.67	91.13	90.73
	Recall (%)	93.91	90.35	91.91
	F1-score (%)	93.79	91.24	90.82

Table 5 demonstrates the performance analysis of the suggested YPALDC model on SN-AM, MiMM_SBILab, and C-NMC datasets with and without hyperparameter modification. Without tuning, the YPALDC model demonstrates strong baseline performance; however, after applying grid search for hyperparameter optimization, noticeable improvements are observed in all key metrics. The model's decision bounds are fine-tuned by optimization on the SN-AM dataset, leading to improved reliability on structured clinical data. For the MiMM_SBILab and C-NMC datasets, which include more challenging and diverse image conditions, tuning significantly enhances the model's generalization. Overall, this proves that optimizing YPALDC's hyperparameters is crucial for improving its performance on different types of medical datasets.

V. CONCLUSION

This study proposes the YPALDC technique to demonstrate effective classification and detection of leukemia using modified YOLOv8 architecture combined with a new PLFOECAM. The advanced preprocessing techniques was applied to enhance the image quality. DWSCNN improves the feature extraction while reducing complexity. RCBAM enhances attention to clinically relevant regions in blood smear images. PLFOECAM replaces gradient-based CAMs with stable, entropy-driven attention maps for better interpretability. Overall, the model achieves robust performance, real-time detection and transparent decision-making in leukemia classification. Finally, the experimental results prove that the proposed model perform achieves 93.85%, 90.42% and 91.87% on SN-AM dataset, MiMM_SBILab Dataset, C-NMC dataset outperforming other standard models.

REFERENCES

[1] A. S. Davis, A. J. Viera, and M. D. Mead, "Leukemia: an overview for primary care," *American Family Physician*, *vol. 89, no. 9*, pp. 731-738, 2014.

[2] I. González-Herrero, G. Rodríguez-Hernández, A. Luengas-Martínez, M. Isidro-Hernández, R. Jiménez, M. B. García-Cenador, et al., "The making of leukemia," *International Journal of Molecular Sciences*, *vol. 19, no. 5*, p. 1494, 2018.

[3] O. O. Odejide, D. Y. Salas Coronado, C. D. Watts, A. A. Wright, and G. A. Abel, "End-of-life care for blood cancers: a series of focus groups with hematologic oncologists," *Journal of Oncology Practice*, *vol. 10, no. 6*, pp. e396-e403, 2014.

[4] J. H. C. Chang, M. M. Poppe, C. H. Hua, K. J. Marcus, and N. Esiashvili, "Acute lymphoblastic leukemia," *Pediatric Blood & Cancer*, *vol. 68*, p. e28371, 2021.

[5] H. Döhner, D. J. Weisdorf, and C. D. Bloomfield, "Acute myeloid leukemia," *New England Journal of Medicine*, *vol. 373, no. 12*, pp. 1136-1152, 2015.

[6] P. Ghia, A. J. Ferreri, and F. Caligaris-Cappio, "Chronic lymphocytic leukemia," *Critical Reviews in Oncology/Hematology*, *vol. 64, no. 3*, pp. 234-246, 2007.

[7] A. Quintás-Cardama and J. E. Cortes, "Chronic myeloid leukemia: diagnosis and treatment," *Mayo Clinic Proceedings*, *vol. 81, no. 7*, pp. 973-988, Jul. 2006.

[8] C. K. Tebbi, "Etiology of acute leukemia: A review," *Cancers*, *vol. 13, no. 9*, p. 2256, 2021.

[9] L. N. Toksvang, S. H. Lee, J. J. Yang, and K. Schmiegelow, "Maintenance therapy for acute lymphoblastic leukemia: basic science and clinical translations," *Leukemia*, *vol. 36, no. 7*, pp. 1749-1758, 2022.

[10] G. Wagner, K. Fenchel, W. Back, A. Schulz, and M. M. Sachse, "Leukemia cutis–epidemiology, clinical presentation, and differential diagnoses," *JDDG: Journal der Deutschen Dermatologischen Gesellschaft*, *vol. 10, no. 1*, pp. 27-36, 2012.

[11] C. Yu, Y. Y. Peng, L. Liu, X. Wang, and Q. Xiao, "Leukemia can be effectively early predicted in routine physical examination with the assistance of machine learning models," *Journal of Healthcare Engineering*, *vol. 2022, no. 1*, p. 8641194, 2022.

[12] M. A. Hossain, A. M. Islam, S. Islam, S. Shatabda, and A. Ahmed, "Symptom based explainable artificial intelligence model for leukemia detection," *IEEE Access*, *vol. 10*, pp. 57283-57298, 2022.

[13] J. Shreve, M. Meggendorfer, H. Awada, S. Mukherjee, W. Walter, S. Hutter, et al., "A personalized prediction model to risk stratify patients with acute myeloid leukemia (AML) using artificial intelligence," *Blood*, *vol. 134*, p. 2091, 2019.

[14] S. Malik, A. Iftikhar, F. H. Tauqeer, M. Adil, and S. Ahmed, "A systematic literature review on leukemia prediction using machine learning," *Journal of Computing & Biomedical Informatics*, *vol. 3, no. 2*, pp. 104-123, 2022.

[15] A. Saeed, S. Shoukat, K. Shehzad, I. Ahmad, A. A. Eshmawi, A. H. Amin, and E. Tag-Eldin,

"A deep learning-based approach for the diagnosis of acute lymphoblastic leukemia," *Electronics*, *vol. 11, no. 19*, p. 3168, 2022.

[16] R. Raina, N. K. Gondhi, Chaahat, D. Singh, M. Kaur, and H. N. Lee, "A systematic review on acute leukemia detection using deep learning techniques," *Archives of Computational Methods in Engineering*, *vol. 30, no. 1*, pp. 251-270, 2023.

[17] A. I. Shehta, M. Nasr, and A. E. D. M. El Ghazali, "Blood cancer prediction model based on deep learning technique," *Scientific Reports*, *vol. 15, no. 1*, p. 1889, 2025.

[18] P. Manescu, P. Narayanan, C. Bendkowski, M. Elmi, R. Claveau, V. Pawar, et al., "Automated detection of acute promyelocytic leukemia in blood films and bone marrow aspirates with annotation-free deep learning," *arXiv preprint* arXiv:2203.10626, 2022.

[19] I. A. Ahmed, E. M. Senan, H. S. A. Shatnawi, Z. M. Alkhraisha, and M. M. A. Al-Azzam, "Hybrid techniques for the diagnosis of acute lymphoblastic leukemia based on fusion of CNN features," *Diagnostics*, *vol. 13, no. 6*, p. 1026, 2023.

[20] G. Yan, M. Gu, S. Wei, H. Li, L. Qiu, A. Liu, et al., "Diagnosis and typing of leukemia using a single peripheral blood cell through deep learning," *Cancer Science*, *vol. 116, no. 2*, pp. 533-543, 2025.

[21] L. Boldú, A. Merino, A. Acevedo, A. Molina, and J. Rodellar, "A deep learning model (ALNet) for the diagnosis of acute leukaemia lineage using peripheral blood cell images," *Computer Methods and Programs in Biomedicine*, *vol. 202*, p. 105999, 2021.

[22] K. D. Prakash, J. Khan, and K. Kim, "Lightweight and efficient YOLOv8 with residual attention mechanism for precise leukemia detection and classification," *IEEE Access*, 2024.

[23] T. O. Asar and M. Ragab, "Leukemia detection and classification using computer-aided diagnosis system with falcon optimization algorithm and deep learning," *Scientific Reports*, *vol. 14, no. 1*, p. 21755, 2024.

[24] A. Awad and S. A. Aly, "Early diagnosis of acute lymphoblastic leukemia using YOLOv8 and YOLOv11 deep learning models," *arXiv preprint* arXiv:2410.10701, 2024.

[25] M. Awais, M. N. Abdal, T. Akram, A. Alasiry, M. Marzougui, and A. Masood, "An efficient decision support system for leukemia identification utilizing nature-inspired deep feature optimization," *Frontiers in Oncology*, *vol. 14*, p. 1328200, 2024.

[26] M. H. A. M. H. Himel, M. A. M. Hasan, T. Suzuki, and J. Shin, "Feature fusion based ensemble of deep networks for acute leukemia diagnosis using microscopic smear images," *IEEE Access*, 2024.

[27] T. R. Mahesh, D. Santhakumar, A. Balajee, H. S. Shreenidhi, V. V. Kumar, and J. R. Annand, "Hybrid ant lion mutated ant colony optimizer technique with particle swarm optimization for leukemia prediction using microarray gene data," *IEEE Access*, *vol. 12*, pp. 10910-10919, 2024.

[28] K. D. Shree and S. Logeswari, "ODRNN: Optimized deep recurrent neural networks for automatic detection of leukaemia," *Signal, Image and Video Processing*, *vol. 18, no. 5*, pp. 4157-4173, 2024.

[29] H. Almahdawi, A. Akbas, and J. Rahebi, "Deep learning neural network based on PSO for leukemia cell disease diagnosis from microscope images," *Journal of Imaging Informatics in Medicine*, pp. 1-10, 2025.

[30] M. Dutta, M. U. Mojumdar, M. A. Kabir, N. R. Chakraborty, S. M. T. Siddiquee, and S. Abdullah, "LEU3: An attention augmented-based model for acute lymphoblastic leukemia classification," *IEEE Access*, 2025.

[31] A. Thiriveedhi, S. Ghanta, S. Biswas, and A. K. Pradhan, "ALL-Net: integrating CNN and explainable-AI for enhanced diagnosis and interpretation of acute lymphoblastic leukemia," *PeerJ Computer Science*, *vol. 11*, p. e2600, 2025.

[32] J. Maus, P. Nikulin, F. Hofheinz, J. Petr, A. Braune, J. Kotzerke, and J. van den Hoff, "Deep learning based bilateral filtering for edge-preserving denoising of respiratory-gated PET," *EJNMMI Physics*, *vol. 11, no. 1*, p. 58, 2024.

[33] D. Onder, S. Zengin, and S. Sarioglu, "A review on color normalization and color deconvolution methods in histopathology," *Applied Immunohistochemistry & Molecular Morphology*, *vol. 22, no. 10*, pp. 713-719, 2014.

[34] P. Härtinger and C. Steger, "Adaptive histogram equalization in constant time," *Journal of Real-Time Image Processing*, *vol. 21, no. 3*, p. 93, 2024.

[35] N. Fei, Y. Gao, Z. Lu, and T. Xiang, "Z-score normalization, hubness, and few-shot learning," in *Proc. IEEE/CVF Int. Conf. Computer Vision*, pp. 142-151, 2021.

[36] E. Tadmor, "Entropy stability theory for difference approximations of nonlinear conservation laws and related time-dependent

problems," *Acta Numerica*, *vol. 12*, pp. 451-512, 2003.

[37] "The Cancer Imaging Archive Wiki,"(Available)https://wiki.cancerimagingarchive.net/pages/viewpage.action?pageId=52757009.

[38] "MIMM SBILab Collection - Cancer Imaging Archive,"(Available):https://www.cancerimagingarchive.net/collection/mimm_sbilab/.

[39] "C-NMC-2019 Collection - Cancer Imaging Archive,"(Available):https://www.cancerimagingarchive.net/collection/c-nmc-2019/.